VPSC Implementation in BISON-CASL Code for Modeling Large Deformation Problems
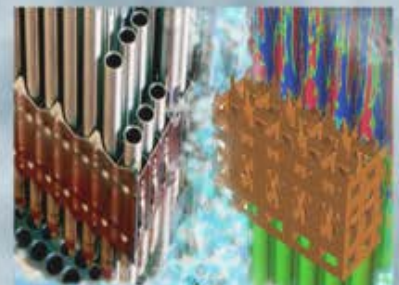
Wenfeng Liu
ANATECH Corporation

Robert Montgomery
Pacific Northwest National Laboratory

Carlos Tomé and Chris Stanek
Los Alamos National Laboratory

Jason Hales
Idaho National Laboratory

April 19, 2015

U.S. DEPARTMENT OF ENERGY | Nuclear Energy

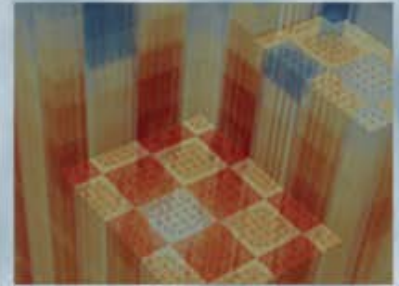# VPSC IMPLEMENTATION IN BISON-CASL CODE FOR MODELING LARGE DEFORMATION PROBLEMS

Wenfeng Liu
ANATECH Corp.
5435 Oberlin Dr., San Diego, CA 92121
wenfeng.liu@anatech.com

Robert Montgomery
Pacific Northwest National Laboratory
robert.montgomery@pnnl.gov

Carlos Tomé and Chris Stanek
Los Alamos National Laboratory
tome@lanl.gov, stanek@lanl.gov

Jason Hales
Idaho National Laboratory
jason.hales@inl.gov

ABSTRACT

This paper describes a multi-scale modeling approach to compute the large-strain deformation of zirconium alloy cladding, which is of interest to the study of fuel rod behaviors in transient and accident conditions. A Visco-Plastic Self-Consistent (VPSC) polycrystal plasticity model representing polycrystals by weighted orientations of single crystals has been implemented as the constitutive law in a finite element fuel code BISON-CASL to model the deformation of α-phase zirconium alloy cladding. Result of a benchmark test case has verified the functionality of the VPSC model in the BISON-CASL code. A demonstration case representing the geometry of a segment of cladding tube under constant rod internal pressure and imposed temperature ramp was prepared to simulate the thermal and mechanical loads in a postulated LOCA condition, and the case has been tested using BISON-CASL. Results have demonstrated the code's capability of modeling of large localized deformation of cladding tube due to temperature variation in a postulated LOCA condition.

Key Words: VPSC, Ballooning, LOCA

1   INTRODUCTION

In transient and accident conditions, large deformation of fuel cladding tube may occur. This needs to be accurately modeled in a fuel performance code to predict the fuel rod behavior. In the instance of a postulated LOCA, the conditions external to the fuel rod lead to significant heat up of the cladding (Cladding temperatures can range from 600°C to 1200°C, depending on a variety of factors.) and decrease in coolant pressure. Under these conditions, thermal creep and plastic deformation of the cladding can lead to large strain accumulation, a phenomenon called ballooning. Clad ballooning is important during a LOCA since:

    a) The cladding expansion would cause reduction of flow area and blockage of the coolant channel, adversely impacting the coolant flow and heat transfer conditions [1]. This has

become a regulatory requirement that changes in core geometry shall be such that the core remains amenable to cooling, and the long term cooling capability shall be maintained.

b) Clad ballooning creates additional room between clad and fuel pellets, which allows the axial relocation of fuel fragments into the ballooned region and increases the local heat generation.

c) Clad ballooning may lead to the clad rupture and allows the release of fission products into the environment.

Typically, transient fuel behavior modeling is used to calculate the cladding deformation during high temperature ballooning in order to account for the impact of irradiation on rod internal pressure and the fuel stored energy. Empirical correlations for the mechanical properties of zirconium alloys have been used in engineering fuel codes such as Falcon to estimate the burst stress and burst strain data as a method to calculate cladding deformation and flow blockage potential [2][3]. Such an approach, however, lacks a mechanistic understanding of the microstructural processes that control thermal creep and fracture of zirconium alloys under high temperature conditions representative of a LOCA.

The Visco-Plastic Self-Consistent (VPSC) polycrystal plasticity modeling approach, developed by Lebensohn and Tomé [4], accounts for the mechanistic material processes controlling the deformation behavior of zirconium alloys. In brief: metallic materials are formed by crystallographic domains called grains. Within VPSC the metallic aggregate (polycrystal) is represented by weighted orientations of single crystals, representing a grain and its associated volume fraction, respectively. The response and properties of such aggregate are given by averaging the response and the properties of the individual constituent grains. VPSC keeps track of the stress, strain, crystal orientation, activity and activation stress in each slip system in each grain, dislocation density on each slip system, etc. Incorporating such a material behavior model into a finite element code is important to capture the anisotropic nature of deformation of zirconium alloy cladding at high temperatures.

This paper presents a multi-scale modeling approach under development that couples the VPSC model to an engineering scale code BISON-CASL (formerly known as Peregrine [5]). Section 2 describes the VPSC model as a constitutive law for modeling the deformation of α-phase zirconium alloy and the numerical procedure to implement the VPSC model in the BISON-CASL code. Section 3 presents results of a benchmark case to verify the implementation of the material model by comparing the BISON-CASL result to the standalone VPSC result. Section 3 also gives result of a demonstration case that represents a segment of cladding tube under constant internal pressure and imposed temperature ramp. The results have demonstrated the capability of the code to model large-strain localized deformation caused by small axial temperature variations. Therefore, it provides the capability of modeling the clad ballooning during postulated LOCA coolant blowdown and heat-up conditions. Emphasis has been placed upon testing the functionality to model the large deformation behavior; benchmarking material property parameters at high temperatures are still considered necessary when measurement data become available.

2 METHODOLOGY

2.1 Visco Plastic Self Consistent Model

The fully anisotropic VPSC polycrystal plasticity model was originally developed by Lebensohn and Tomé [2] and has seen continuous improvements since then. VPSC treats each grain as an ellipsoidal visco-plastic inclusion embedded in an effective visco-plastic medium. Both, inclusion and medium have fully anisotropic properties. The effective medium represents the 'average' environment 'seen' by each grain. When boundary conditions of stress or strain rate are applied to the effective medium, an interaction between medium and grain (embedded inclusion) takes place, and local stresses are induced in the inclusion and its vicinity, which drive the deformation of the inclusion. The stresses, which follow from solving the stress equilibrium equations, are uniform inside the inclusion but deviate from the average stress in the medium depending on the relative properties of medium and inclusion. The 'self consistency' of the approach relies on enforcing the condition that the average stress and strain rate over all the grains has to be equal to the boundary values imposed on the medium.

The propagation of slip dislocations induces plastic shear and no volumetric dilatation. Denoting n^s the normal to the slip plane, and b^s the direction of shear (Burgers vector), the resolved shear stress on the shear plane and along the shear direction associated with the stress tensor σ_{ij}^c acting on the grain is given by [1]

$$\tau_{res}^s = b_i^s n_j^s \sigma_{ij}^c = m_{ij}^s \sigma_{ij}^c \tag{1a}$$

where
$$m_{ij}^s = \tfrac{1}{2}(b_i^s n_j^s + b_j^s n_i^s) \tag{1b}$$

is the Schmid tensor that projects the stress along the shear plane. The strain rate tensor associated with shear rate $\dot{\gamma}^s$ in system s is

$$\dot{\varepsilon}_{ij} = m_{ij}^s \dot{\gamma}^s \tag{1c}$$

The strain rate associated with climb of forest and loop dislocation segments is given by [6]

$$\dot{\varepsilon}_{ij}^{(climb)} = sym\left(\sum_s \rho^s (\hat{t}^s \otimes \overline{v}^s)_i b_j^s \right) \tag{2a}$$

Where ρ^s is the density of segments 's', v^s is their climb velocity, b^s is their Burgers vector, t^s is their tangent vector. In the case of climb only the edge component of the dislocation matters. If we assume that all dislocations are pure edge Eq (2a) becomes

$$\dot{\varepsilon}_{ij}^{(climb)} = sym\left(\sum_s \rho^s v^s b^s \hat{b}_i^s \hat{b}_j^s \right) \tag{2b}$$

For describing creep we use a power law in which the shear rates are given by a power of the ratio between resolved shear stress and a threshold stress

---

[1] Unless stated otherwise, throughout this text we use the implicit summation convention: repeated indices in equations denote summation over the range of such indices.

$$\dot{\gamma}^s = \dot{\gamma}_o \left(\frac{m_{kl}^s \, \sigma_{kl}}{\tau_{thres}^s} \right)^n \tag{3}$$

Here $\dot{\gamma}_o$ is a normalization factor and n is the rate-sensitivity exponent. When several systems are active in a grain, the strain rate is given by the sum of their shear rates

$$\dot{\varepsilon}_{ij} = \sum_s m_{ij}^s \, \dot{\gamma}^s = \dot{\gamma}_o \sum_s m_{ij}^s \left(\frac{m_{kl}^s \, \sigma_{kl}}{\tau_{thres}^s} \right)^n \tag{4}$$

Linearizing Eq. (4) inside the domain of a grain gives:

$$\dot{\varepsilon}_{ij} = M_{ijkl}(\sigma)\, \sigma_{kl} + \dot{\varepsilon}_{ij}^o + \dot{\varepsilon}_{ij}^{growth} \tag{5}$$

where M_{ijkl} and ε_{ij}^o are the viscoplastic compliance and the back-extrapolated term for a given grain, respectively. The linearization of the constitutive response is required to solve the equilibrium conditions between inclusion and medium, and is actually a tangent approximation to the non-linear law Eq. (4). In Ref. [7], we have shown that irradiation creep, thermal creep, and instantaneous plasticity can be expressed in the form of Eq. (4). In Eq. (5) a stress-independent extra term is added in order to account for the irradiation growth rate of the grain. The constitutive law giving the response of the effective medium (polycrystal) is given by a linear relation analogous to Eq. (5):

$$\bar{\dot{\varepsilon}}_{ij} = \bar{M}_{ijkl} \, \bar{\sigma}_{kl} + \bar{\dot{\varepsilon}}_{ij}^o \tag{6}$$

where $\bar{\dot{\varepsilon}}_{ij}$ and $\bar{\sigma}_{kl}$ are overall (macroscopic) magnitudes and $\bar{M}_{ijkl}$ and $\bar{\dot{\varepsilon}}_{ij}^o$ are the macroscopic visco-plastic compliance and back-extrapolated rate, respectively. The growth of the polycrystal cannot be separated from the back-extrapolated parameter and the term $\bar{\dot{\varepsilon}}_{ij}^o$ accounts for both. The macroscopic moduli are unknown *a priori* and need to be adjusted self-consistently by enforcing the condition that the stress and strain rate averaged over all grains has to be equal to the stress and strain rate of the effective medium

$$\bar{\dot{\varepsilon}}_{ij} = \left\langle \dot{\varepsilon}_{ij}^c \right\rangle \quad and \quad \bar{\sigma}_{kl} = \left\langle \bar{\sigma}_{kl}^c \right\rangle \tag{7}$$

In the current application to high temperature, high stress conditions, thermal creep is considered as the dominating deformation mechanism. In zirconium alloys, thermal creep principally occurs by glide of dislocations overcoming obstacles via stress and temperature activated mechanisms of diffusion. As such, thermal creep is relevant at high temperatures ($T > 0.5 T_M$) or at applied stresses approaching the flow stress ($\sigma > 0.75\, \sigma_F$). The viscous power law expressed by Eq. (4) is appropriate for describing the contribution of several slip systems to the thermal creep in a grain

$$\dot{\varepsilon}_{ij}^{thermal} = \sum_s m_{ij}^s \, \dot{\gamma}^s = \dot{\gamma}_o(T) \sum_s m_{ij}^s \left(\frac{m_{kl}^s \, \sigma_{kl}}{\tau_{thres}^s} \right)^4 \tag{8}$$

Dislocation glide is assumed to take place along the prism, basal and pyramidal planes. The parameters that enter into Eq. (8) are related to physical properties of Zr alloys. The parameters used in VPSC were derived by Ref. [8] by fitting a comprehensive database of tensile and shear

creep experiments performed on Zr-2.5%Nb alloy tubes, at different temperatures, and imposing various uniaxial and bi-axial stress states. Their expression assumes that $\dot{\gamma}_o$ is the same for all systems with $\dot{\gamma}_0 = \dot{\gamma}_0(T = 523)\exp\left[-Q(1/T - 1/523)\right]$. Where, $\dot{\gamma}_0(T = 523) = 4.157 \times 10^{-3} h^{-1}$ and $Q(T) = \left(5000 + \dfrac{5600}{1 + \exp(-(T - 470)/15)}\right)$. The reference shear rate $\dot{\gamma}_o$ depends on temperature and the activation energy for the diffusion controlled mechanism. The threshold stresses in Eq (8) that fit the experimental data are τ_{thres}^s =0.100, 0.111, 0.300 GPa for prism, basal, and pyramidal glide, respectively. The temperature range covered by the experiments is 373 K <T <596 K, and as such, these threshold shear stress values may not be appropriate for simulating high temperature deformation mechanisms. At high temperatures, the microstructure material model parameters in Eq. (8) need to be re-calibrated. For the purpose of this demonstration, the approach taken for modeling viscoplastic deformations at high temperature is to use an ad-hoc value in the activation energy for $\dot{\gamma}_o$ in place of what has been reported in Ref. [8].

2.2 Interface with BISON-CASL

Finite element solution of a mechanical problem involves solving the weak-form equation of the mechanical equilibrium condition. In the BISON-CASL code, which is based on the MOOSE and BISON code systems [9,10], the global residual associated with the weak-form equation is minimized using a variant of the Newton iteration method. To solve the nonlinear deformation problem which involves creep and plasticity, the increment of total strain at each time step is passed to a material model which would compute a trial stress tensor. The trial stress tensor would be used to update the weak form solution until the convergence is reached, i.e., both the weak-form equilibrium equation and the constitutive relationship between stress and strain are satisfied. Such a computational process requires the VPSC model to compute a stress tensor for the increment of total strain. The calculation of the stress at each integration point involves a second, local Newton iteration to solve for the trial stress tensor.

At each time step, knowing the old stress tensor at time t, the problem is to provide an update of the trial stress, the stress computed using the increment of total strain regardless of the code's convergence, at current time t+Δt as shown in following equations.

$$\sigma_{t+\Delta t} = \sigma_t + C\Delta\varepsilon_e \qquad (9)$$
$$\Delta\varepsilon_e = \Delta\varepsilon - \Delta\varepsilon_p \qquad (10)$$

where,

σ_t is the old stress tensor at time t

C is the elastic stiffness tensor of the polycrystal

$\Delta\varepsilon_e$ is the elastic strain increment at time t

$\Delta\varepsilon$ is the total strain increment at time t

$\Delta\varepsilon_p$ is the plastic strain increment computed in VPSC

The residual, R in Eq. (11), as a function of the trial stress is defined as the difference between the sum of the elastic strain increment and the plastic strain increment and the total strain increment computed by BISON-CASL.

$$R = C^{-1}\Delta\sigma + \Delta t\dot{\varepsilon}_p - \Delta\varepsilon_t \qquad (11)$$

where,

$$\Delta\sigma = \sigma_{t+\Delta t} - \sigma_t$$

$\Delta\varepsilon_t$ is the total strain increment computed by BISON-CASL

$$\Delta t \dot{\varepsilon}_p \equiv \Delta\varepsilon_p$$

Newton iteration method is used to compute the trial stress.

$$\Delta\sigma_{k+1} = \Delta\sigma_k - \frac{\partial R}{\partial\Delta\sigma_k} R(\Delta\sigma_k) \tag{12}$$

Subscript k represents the k_{th} iteration in the local Newton iteration loop to compute the trial stress.

The convergence is determined by following quantities.

$$e_1 = \left| \Delta\varepsilon_t - \Delta\varepsilon_p(\sigma_{tr}) - \Delta\varepsilon_e(\sigma_{tr}) \right| \tag{13}$$

$$e_2 = \left| \Delta\varepsilon_t - \Delta\varepsilon_p(\sigma_{tr}) - \Delta\varepsilon_e(\sigma_{tr}) / |\Delta\varepsilon_t\| \right| \tag{14}$$

$$e_3 = \left| \Delta\varepsilon_{t,k} - \Delta\varepsilon_{p,k}(\sigma_{tr,k}) - \Delta\varepsilon_{e,k}(\sigma_{tr,k}) | / | \Delta\varepsilon_{t,1} - \Delta\varepsilon_{p,1}(\sigma_{tr,1}) - \Delta\varepsilon_{e,1}(\sigma_{tr,1}) \right\| \tag{15}$$

where,

σ_{tr} is the trial stress computed in VPSC,

$\Delta\varepsilon_t$ is the total strain increment,

$\Delta\varepsilon_e$ is the elastic strain increment,

$\Delta\varepsilon_p$ is the plastic strain increment,

In the iteration loop, convergence is detected if either of the three quantities are lower than prescribed tolerances, which were specified in the input. If a prescribed maximum number of iteration is reached but none of these quantities are lower than prescribed tolerances, the code is considered to be diverged and stops running. Note that the present discussion of convergence is only limited to the interface that couples VPSC and the BISON-CASL code.

A typical VPSC texture can have a few thousand orientations, which would incur significant computational cost when implemented in the finite element code. To optimize running times of BISON-CASL, reduced number of orientations is used to represent the texture. Study has found that using the four-grain texture gives deviation of ~5% in the computed strains in comparison to the ones of 1944 grain texture [7]. The four-grain texture has been used in the test cases in current paper.

3   RESULTS

3.1 Benchmark Case

A benchmark case using a single element was prepared to test if the capabilities of modeling of large deformation have been implemented correctly in the BISON-CASL code. Under prescribed load conditions, the standalone-VPSC can compute the material response of a single element, which can be used to compare with the results from the VPSC model implemented in the BISON-CASL code. Key input parameters are shown in Table I.

Table I. Key input parameters for the benchmark case

Parameter	Unit	Value
Stress (in X direction)	MPa	200
Temperature	K	1073
Texture described using Euler angles*		(136.83, 80.30, 0.0) (136.83, 99.70, 0.0) (221.37, 80.30, 0.0) (221.37, 99.70, 0.0)

* The texture describes the fraction of crystals with a given orientation in terms of Euler angles of three consecutive rotations: a) The first is the angle of rotation around the sample axis Z; b) The second is the angle of rotation around the rotated crystal axis X; c) The third is the angle of rotation around the crystal axis Z in the new coordinate system. 4-grain texture has been used for this test case.

The comparison of the plastic strains between BISON-CASL and standalone VPSC is shown in Figure 1. The agreement between the standalone VPSC results and those obtained using the finite element formulation and coupling approach verifies that the coupling methodology functions as designed. At 28 hr, the difference of the calculated plastic strains between the standalone VPSC and BISON-CASL is less than 0.001. Figure 2 shows the true strain computed using the displacement output in comparison with the strain output from the BISON-CASL code, which verifies the correct computation of large strain using BISON-CASL.
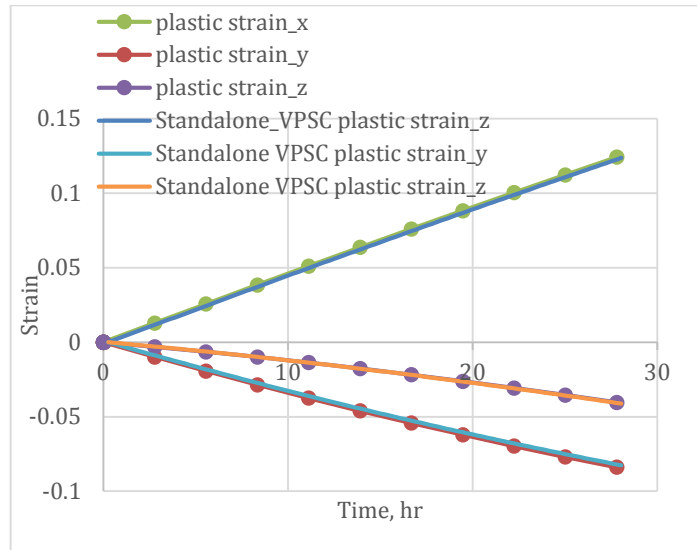

Figure 1 Comparison between BISON-CASL and standalone VPSC on modeling high temperature creep of four-grain polycrystal
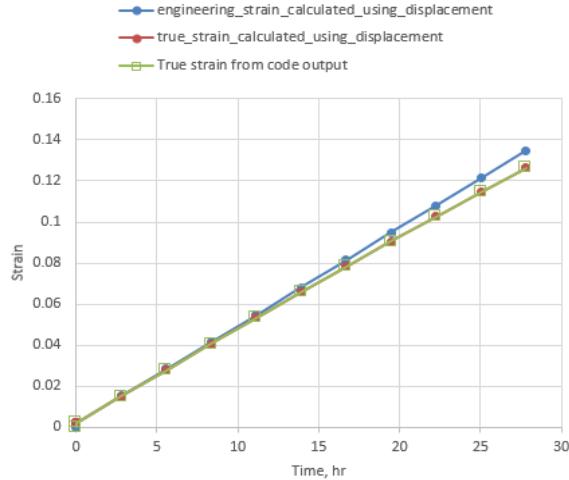
Figure 2 Comparison between the true strain from code output (standalone VPSC), the engineering strain obtained from BISON-CASL coupling, and the true strain computed using displacements from BISON-CASL

3.2 Ballooning Demonstration

A test case to model a segment of axially-constrained clad tube was prepared to evaluate the capability BISON-CASL/VPSC coupling to simulate large-strain deformation leading to clad ballooning during a LOCA. As has been described in Section 2.1, the material parameters for the high temperature application is applicable up to 596 K, which is below the simulated temperatures of interest to LOCA. Therefore, for current demonstration purpose, an ad-hoc change in the activation energy is used to artificially increase the creep rate. The key input parameters are provided in Table I and Figure 3.

Table I. Key input parameters for the ballooning test case

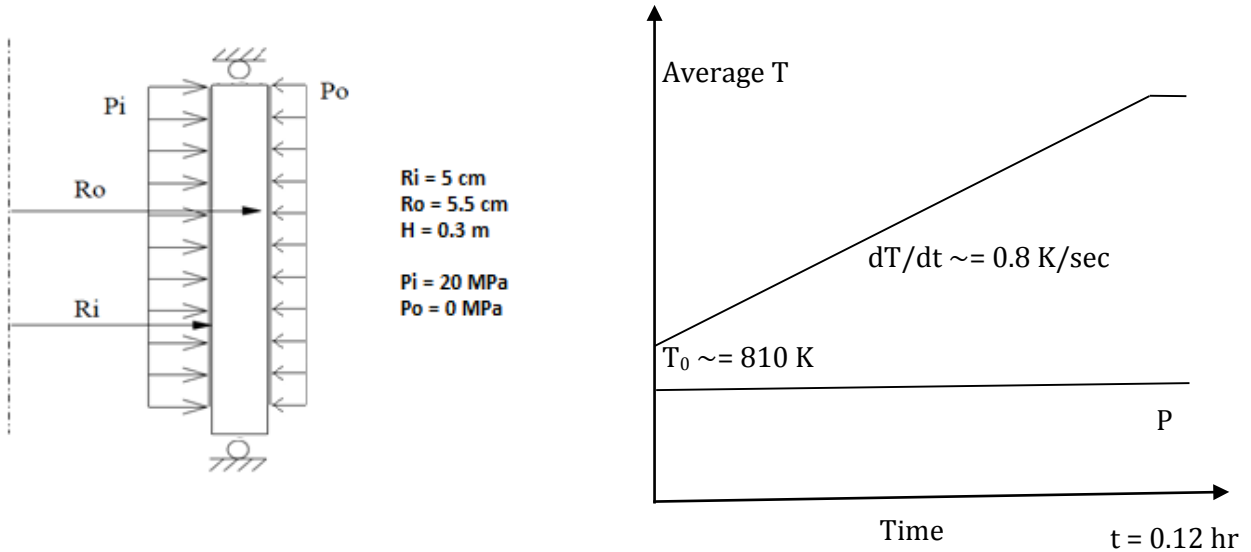| Parameter	Unit	Value
Number of elements	-	5
Element type	-	QUAD4 axisymmetric
Internal pressure	MPa	20
External pressure	MPa	0
Texture	-	Four-grain
Time dependent average temperature	K	810-1073
Simulation time	hr	0.12
Peak (temperature) to average ratio	-	1.012
Q/R (Activation energy in Eq. 8)	K	18,000

Figure 3 Schematic of input conditions for testing high temperature creep

The boundary and initial conditions consist of a constant pressure of 20 MPa on the inside surface of the tube and an applied average temperature ramp of 0.8 K/sec starting at an initial temperature of 810 K. The mechanical boundary conditions at the top and bottom of the tube only allow for radial displacements, with no axial expansion or contraction occurring during the simulation. These mechanical constraints result in a biaxial stress state within the tube with an axial stress that is much larger than a closed tube condition ($\sigma_{axial} = \frac{1}{2}\sigma_{hoop}$). A peak-to-average temperature ratio of 1.012 is applied at the tube mid-height. This temperature profile produces a 30°C temperature variation in the axial direction.

Results of the total hoop, axial, and radial strains computed using BISON-CASL are shown in Figure 4. The results demonstrate a significant amount of wall thinning as represented by the equal amount of strain in the hoop and radial directions ($\varepsilon_{hoop} \approx \varepsilon_{radial}$). The wall thinning is further observed in Figure 5 which shows the deformed geometry at the end of simulation under the imposed axial temperature profile. Figure 6 shows the comparison of the hoop strain between the mid-height element with the largest deformation and the top element with relatively smaller deformation.

The large deformation can be simulated due to accumulated creep strains in the whole segment of the cladding tube under rod internal pressure. The initial difference in deformation between the mid-height element with higher temperature and top/bottom element with lower temperature is small; the major difference is due to different creep rates at different temperatures. When the deformation becomes large (hoop strain > 5%), both the temperature and the deformed geometry contribute to the deformation rate. This result is consistent with experimental data obtained by Erbacher, et al. who demonstrated that azimuthal temperature variations of ~25 K are sufficient to reduce the circumferential average ballooning strain by a factor of 2 [11].
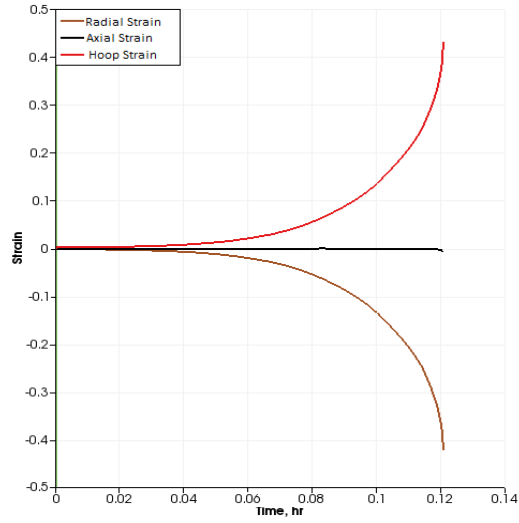
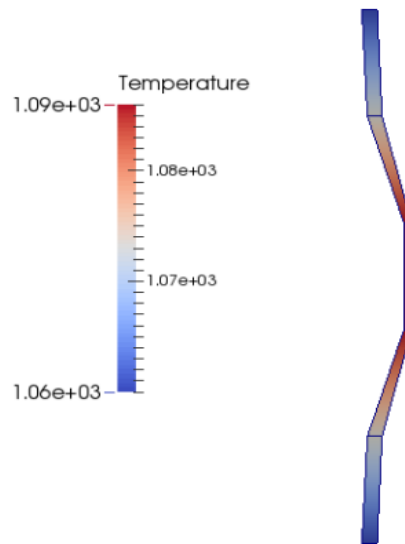**Figure 4 Total strains versus time at the mid-height element**

Figure 5 Temperature contour and deformed geometry at the end of simulation (Aspect ratio scaled 20x)
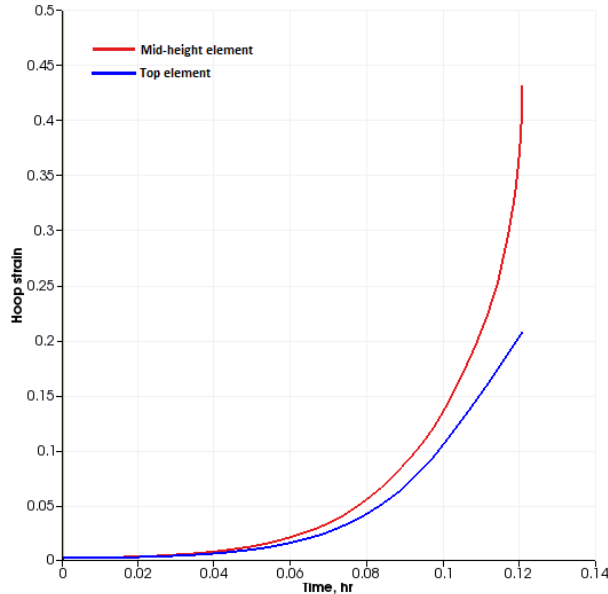
Figure 6 Comparison of hoop strain between the mid-height element and the top element

The higher temperature at the mid-height element promotes a higher creep rate that results in more localized radial deformation. To conserve volume, the tube wall must also deform, resulting in wall thinning. The mid-height segment with higher temperature (1086 K @ 0.12 hr) has more than 40% cladding wall thickness reduction as compared to the 20% cladding wall thickness reduction at the top and bottom segments with relatively lower temperature (1060-1073 K @ 0.12 hr). Under constant pressure load, the true hoop stress increases as a result of the cladding wall thinning (area reduction), which in turn contributes to a higher creep rate. This positive feedback mechanism leads to rapid deformation rates that cause rupture of the cladding. This case has demonstrated that a small temperature difference (<30 K) is sufficient to cause large localized deformation and subsequent clad ballooning.

4   CONCLUSIONS

This paper describes a multi-scale modeling approach to calculate the large-strain deformation of zirconium alloy cladding. A VPSC model based on averaging the deformation in single crystals at different orientations is used as the constitutive law for modeling the deformation of α-phase zirconium. The VPSC model is implemented in the engineering scale fuel code BISON-CASL to model the deformation of polycrystalline α-phase zirconium. Benchmark test result has verified the functionality of the VPSC model in the BISON-CASL code. A demonstration case representing the geometry of a segment of cladding tube under constant rod internal pressure and imposed temperature ramp was prepared, and has been tested using BISON-CASL. The test results have demonstrated the capability of mechanistic modeling of large-strain deformation at high temperatures, and, under imposed axial temperature profile, the localized clad thinning (or ballooning) can be simulated.

5 ACKNOWLEDGMENTS

6 REFERENCES

1. H. M. Chung and T. F. Kassner, "Embrittlement Criteria for Zircaloy Fuel Cladding Applicable to Accident Situations in Light-Water Reactors: Summary Report," *NUREG-CR1344*, Argonne National Laboratory, (1980).

2. M. N. Jahingir, J. Alvis, R. O. Montgomery, and O. Ozer, "Analysis of Fuel Behavior During LOCA Tests Using FALCON MOD01," *Proceedings of the 2005 Water Reactor Fuel Performance Meeting*, Kyoto, Japan, October 2-6, (2005).

3. Y. Rashid, R. Dunham, and R. Montgomery, *Fuel Analysis and Licensing Code: Falcon MOD01*: *Volume 1: Theoretical and Numerical Bases*, EPRI, Palo Alto, 1011307, (2004).

4. R. Lebensohn and C.N. Tomé, *Acta Metallurgica et Materialia,* **Vol. 41, No. 9**, (1993).

5. R. O. Montgomery, "Peregrine: Advanced Modeling of Pellet-Cladding Interaction (PCI) Failure in LWRs," *Proceedings of the TopFuel 2012 Reactor Fuel Performance Meeting*, Manchester, U.K., Sep. 2-6, (2012).

6. C. H. Woo, "Polycrystalline Effects on Irradiation Growth and Creep in Textured Zirconium," *Journal of Nuclear Materials,* **Vol. 131,** pp.105, (1985).

7. W. Liu, R. O. Montgomery, and C. N. Tomé, "Demonstration of Atomistically-informed Multiscale Zr Alloy Deformation Models in Peregrine for Normal and Accident Scenarios", CASL-U-2014-201-000, (2014).

8. N. Christodoulou, P.A. Turner, C.N. Tomé, C.K. Chow, and R.J. Klassen, "Analysis of steady-state thermal creep of Zr-2.5%Nb pressure tube material", *Metall. and Material Trans.* **33A** pp.1103-15, (2002).

9. D. Gaston, C. Newman, G. Hansen, and D. Lebrun-Grandié, "MOOSE: A parallel computational framework for coupled systems of nonlinear equations," *Nucl. Eng. Design*, **239**, pp. 1768–1778, (2009).

10. R. L. Williamson, J. D. Hales, S. R. Novascone, M. R. Tonks, D. R. Gaston, C. J. Permann, D. Andrs, and R. C. Martineau, "Multidimensional multiphysics simulation of nuclear fuel behavior," *J. Nucl. Mater.*, **423**, pp. 149—163, (2012).

11. F. J. Erbacher, H.J. Neitzel, H. Rosinger, H. Schmidt, and K. Wiehr, "Burst Criterion of Zircaloy Fuel Claddings in a Loss-of-Coolant Accident," ASTM 754, American Society for Testing and Materials, pp. 271-283, (1982).